

# A New Nonlinear Anisotropic Model for Soft Magnetic Materials

D. Lin, P. Zhou, Z. Badics, W. N. Fu, Q. M. Chen and Z. J. Cendes

**Abstract**—An accurate and efficient nonlinear anisotropic model for soft magnetic materials is developed. In this model, the cross effects of the magnetic field components in different principle directions are decoupled by introducing an equivalent magnitude of the magnetic field in each principle direction based on an anisotropic characterization of the energy density. Only  $B$ - $H$  curves in the principal directions of the materials – two curves in 2D or three curves in 3D – are needed to be measured. The anisotropic behavior of laminations with isotropic or anisotropic steel is also considered. The model is validated by numerical experiments and is applied to the 3D finite element analysis of a synchronous reluctance motor with an axially laminated anisotropic rotor.

**Index Terms**—Axially laminated anisotropic (ALA) rotor, lamination, nonlinear anisotropy, soft magnetic, transient finite element analysis.

## I. INTRODUCTION

WHILE anisotropic behavior is often encountered in electromagnetic devices, current models available to characterize this behavior are inadequate. In particular, the accuracy of basic anisotropic models is poor while attempts to improve the accuracy result in difficult measurement requirements and complex computational representations.

One commonly used model is called the elliptical model [1]. This model derives the permeability of a principal direction directly from the relevant  $B$ - $H$  curve based on the magnitude of the applied magnetic field. If a 2D magnetic field with constant magnitude is applied in different directions, the permeability of each principal direction is constant and, therefore, the vector of the flux density traces an ellipse. However, as reported in [3], this model could not provide a good accuracy.

The co-energy model for grain oriented steels [2] utilizes the stored co-energy density over the  $H_x$ - $H_y$  plane based on four  $B$ - $H$  curves. Two of the curves correspond to the applied field in the two principal directions of the 2D plane, and the other two curves correspond to the  $B$  components in tangent and normal directions to the applied field at  $55^\circ$ . Whenever it is necessary, the flux density  $B$  can be recovered as the gradient of the co-energy density.

Another method of modeling grain oriented steel incorporates a far larger number of magnetization curves [3]. The steel is cut into strips in 10 degree steps with respect to the rolling direction and tested to get  $B$ - $H$  curves in 10 different directions. These curves are then used in the finite element analysis. Obviously, this method has the following drawbacks: (i) the difference in the directions of  $B$  and  $H$  can not be considered, therefore, the method is only suitable for problems where the  $B$  components orthogonal to  $H$  are negligible; (ii) it is not convenient to obtain  $B$ - $H$  curves in so many directions; (iii) it is difficult to expand the method to 3D nonlinear anisotropic problems.

In this paper, a novel model is developed for nonlinear anisotropic soft materials. This model requires only two (for 2D) or three (for 3D)  $B$ - $H$  curves in the principal directions. Such curves may be provided directly by the manufacturers. Furthermore, lamination effects are also considered in the model.

## II. NONLINEAR ANISOTROPIC MODEL

If a magnetic field is applied in a principal direction in a nonlinear anisotropic soft material with negligible hysteresis, the magnitude of the applied magnetic field  $H$  and of flux density  $B$  simply follow the relevant  $B$ - $H$  curve and the directions of  $H$  and  $B$  are the same. However, when  $H$  is applied in any other direction,  $B$  and  $H$  are no longer parallel.

Based on the fact that the application of the same magnitude of  $H$  in different principal directions will cause different level of magnetic saturation, the proposed model refers all components of  $H$  to each principal direction. Thus, an equivalent magnitude of the magnetic field is introduced in each principle direction to consider both the anisotropy and the cross effects of other directions due to nonlinearity. The equivalent magnitudes referred to the  $x$ ,  $y$  and  $z$  directions are computed from

$$\begin{cases} H_e^x = \sqrt{H_x^2 + (k_{xy}H_y)^2 + (k_{xz}k_{\mu z}H_z)^2} \\ H_e^y = \sqrt{(k_{yx}H_x)^2 + H_y^2 + (k_{yz}k_{\mu z}H_z)^2} \\ H_e^z = \sqrt{(k_{zx}H_x)^2 + (k_{zy}H_y)^2 + (k_{\mu z}H_z)^2} \end{cases} \quad (1)$$

For the sake of generality, this model also takes lamination effects into account. We assume in (1) that the steel is laminated in the  $z$  direction. Further,  $k_{\mu z}$  is introduced to consider lamination effects as

Manuscript received Jun 20, 2005.

The authors are with Ansoft Corporation, Pittsburgh, PA 15219 USA (phone: 412-261-3200; e-mail: [dlin@ansoft.com](mailto:dlin@ansoft.com); [ping@ansoft.com](mailto:ping@ansoft.com); [zsolt@ansoft.com](mailto:zsolt@ansoft.com); [wfu@ansoft.com](mailto:wfu@ansoft.com); [chen@ansoft.co.jp](mailto:chen@ansoft.co.jp); [zol@ansoft.com](mailto:zol@ansoft.com)).

$$k_{\mu z} = \frac{\mu_a}{(1-k_{lam})\mu_{fz} + k_{lam}\mu_a} \quad (2)$$

where  $k_{lam}$  is the stacking factor of the lamination. When the steel is not laminated (i.e., solid),  $k_{lam}$  becomes 1. Subscripts ‘‘f’’ and ‘‘a’’ in (2) stand for the iron and insulation parts of the lamination, respectively. The coefficients in (1) are defined as

$$\begin{cases} k_{xy} = 1/k_{yx} = W_m^y / W_m^x \\ k_{xz} = 1/k_{zx} = W_m^z / W_m^x \\ k_{yz} = 1/k_{zy} = W_m^z / W_m^y \end{cases} \quad (3)$$

where the magnetic co-energy densities  $W_m^x$ ,  $W_m^y$  and  $W_m^z$  are obtained from the  $W$ - $H$  curves based on the magnitude  $H_m$  of the applied field  $\mathbf{H}$  as shown in Fig. 1. The  $W$ - $H$  curve in Fig. 1 is derived by integrating the corresponding  $B$ - $H$  curve.

The permeability in each principal direction is obtained in terms of the corresponding equivalent magnetic field magnitudes,  $H_e^x$ ,  $H_e^y$  or  $H_e^z$ . In addition, based on (1), (2)

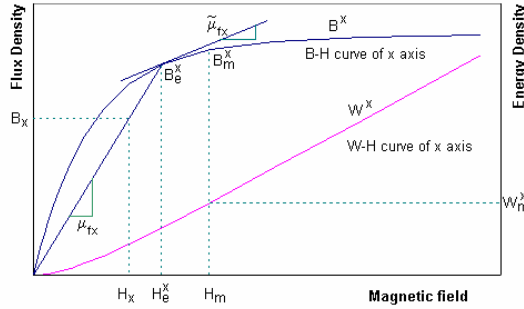


Fig. 1 Permeability and  $W$ - $H$  curve for axis  $x$ . For the other two axes, replace  $x$  by  $y$  or  $z$ .

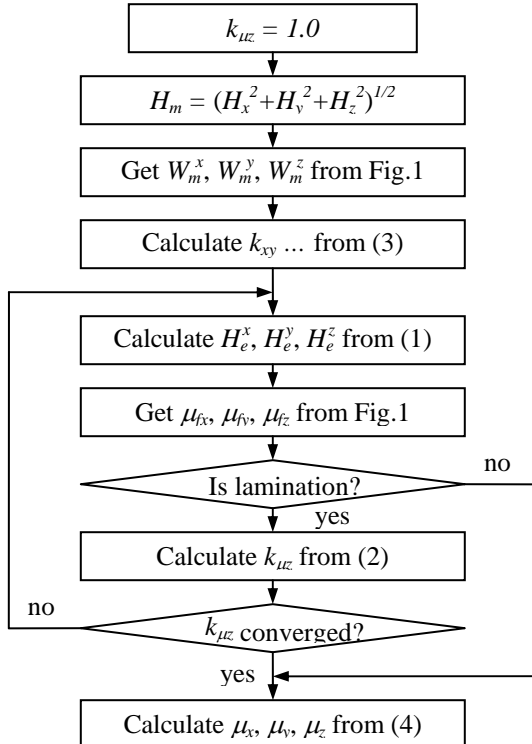


Fig. 2 A simple iterative process to determine  $k_{\mu z}$

and Fig. 1, the coefficient  $k_{\mu z}$  is determined by a simple iterative process, as shown in the flow chart of Fig. 2.

The three components of permeability including lamination effects are

$$\begin{cases} \mu_x = (1-k_{lam})\mu_a + k_{lam}\mu_{fx} \\ \mu_y = (1-k_{lam})\mu_a + k_{lam}\mu_{fy} \\ \mu_z = k_{\mu z}\mu_{fz} \end{cases} \quad (4)$$

and the flux density  $\mathbf{B}$  is calculated from

$$\mathbf{B} = [\mu] \cdot \mathbf{H} \quad (5)$$

where  $[\mu]$  is the permeability tensor

$$[\mu] = \begin{bmatrix} \mu_x & 0 & 0 \\ 0 & \mu_y & 0 \\ 0 & 0 & \mu_z \end{bmatrix}. \quad (6)$$

### III. IMPLEMENTATION IN FEA

The nonlinear anisotropic material model introduced in the previous section is incorporated into a finite element Newton-Raphson iteration scheme where the flux density is computed from

$$\mathbf{B} = \mathbf{B}_0 + [\tilde{\mu}] \cdot (\mathbf{H} - \mathbf{H}_0) \quad (7)$$

where  $\mathbf{B}_0$  and  $\mathbf{H}_0$  denote the previous field solution, and

$$[\tilde{\mu}] = \partial \mathbf{B} / \partial \mathbf{H} = [\Delta \tilde{\mu}] + [\mu]. \quad (8)$$

Note that  $[\Delta \tilde{\mu}]$  in (8) is a full tensor in general. For laminations with anisotropic steel,  $[\Delta \tilde{\mu}]$  can be derived as

$$[\Delta \tilde{\mu}] = \mathbf{A} \cdot \begin{bmatrix} \Delta \tilde{\mu}_{fx} \cdot a_x b_x & \Delta \tilde{\mu}_{fx} \cdot a_x b_y & \Delta \tilde{\mu}_{fx} \cdot a_x b_z \\ \Delta \tilde{\mu}_{fy} \cdot a_y b_x & \Delta \tilde{\mu}_{fy} \cdot a_y b_y & \Delta \tilde{\mu}_{fy} \cdot a_y b_z \\ 0 & 0 & 0 \end{bmatrix} + \mathbf{C} \cdot \begin{bmatrix} \Delta \tilde{\mu}_{fx} \cdot c_x d_x & \Delta \tilde{\mu}_{fx} \cdot c_x d_y & \Delta \tilde{\mu}_{fx} \cdot c_x d_z \\ \Delta \tilde{\mu}_{fy} \cdot c_y d_x & \Delta \tilde{\mu}_{fy} \cdot c_y d_y & \Delta \tilde{\mu}_{fy} \cdot c_y d_z \\ \Delta \tilde{\mu}_{fz} \cdot c_z d_x & \Delta \tilde{\mu}_{fz} \cdot c_z d_x & \Delta \tilde{\mu}_{fz} \cdot c_z d_z \end{bmatrix} \quad (9)$$

where

$$\begin{cases} \Delta \tilde{\mu}_{fx} = \tilde{\mu}_{fx} - \mu_{fx} \\ \Delta \tilde{\mu}_{fy} = \tilde{\mu}_{fy} - \mu_{fy} \\ \Delta \tilde{\mu}_{fz} = \tilde{\mu}_{fz} - \mu_{fz} \end{cases} \quad (10)$$

$$\begin{cases} a_x = \frac{H_x}{k_{xz}} \frac{\partial k_{xz}}{\partial H_m} = -\frac{H_x}{k_{zx}} \frac{\partial k_{zx}}{\partial H_m} \\ a_y = \frac{H_y}{k_{yz}} \frac{\partial k_{yz}}{\partial H_m} = -\frac{H_y}{k_{zy}} \frac{\partial k_{zy}}{\partial H_m} \end{cases} \quad (11)$$

$$\begin{cases} b_x = \partial H_m / \partial H_x = H_x / H_m \\ b_y = \partial H_m / \partial H_y = H_y / H_m \\ b_z = \partial H_m / \partial H_z = H_z / H_m \end{cases} \quad (12)$$

$$\begin{cases} c_x = H_x / H_e^z \\ c_y = H_y / H_e^z \\ c_z = k_{muz}^2 H_z / H_e^z \end{cases} \quad (13)$$

$$\begin{cases} d_x = c_x / k_{xz}^2 - b_x k_{ac} \\ d_y = c_y / k_{yz}^2 - b_y k_{ac} \\ d_z = c_z - b_z k_{ac} \end{cases} \quad (14)$$

and

$$k_{ac} = a_x c_x / k_{xz}^2 + a_y c_y / k_{yz}^2 \quad (15)$$

$$A = k_{lam} \quad (16)$$

$$C = \frac{k_{lam}}{1 + c_z^2 (\Delta \tilde{\mu}_{fz} / \mu_a) (1 - k_{lam}) / k_{\mu z}} \quad (17)$$

For laminations with isotropic steel, where all coefficients in (1) are one, we have

$$a_x = a_y = k_{ac} = 0$$

and

$$d_x = c_x, \quad d_y = c_y, \quad d_z = c_z.$$

Therefore,

$$[\Delta \tilde{\mu}] = C \cdot \Delta \tilde{\mu}_f \begin{bmatrix} c_x^2 & c_x c_y & c_x c_z \\ c_x c_y & c_y^2 & c_y c_z \\ c_x c_z & c_y c_z & c_z^2 \end{bmatrix}. \quad (18)$$

It can be seen from (8) and (18) that for laminations with isotropic steel  $[\tilde{\mu}]$  is a symmetric tensor.

#### IV. VALIDATION

A numerical experiment is set up to validate the proposed model. A nonoriented electrical steel, Armco M-15 with stacking factor of 0.95, is tested with a magnetic field applied in directions  $0^\circ$  ( $x$  axis),  $55^\circ$  (relative to the  $x$  axis towards the  $z$  axis) and  $90^\circ$  ( $z$  axis, i.e., the lamination direction). The results of the numerical experiment published in [4] are shown in Fig.3.

The purpose of this simulation is to see how well the computed results match the experimental data at the critical direction  $55^\circ$  compared to the numerical experiment data at  $0^\circ$  and  $90^\circ$  [2], [3]. Since lamination effects are taken into account in these two curves, the lamination is treated as a solid steel with  $k_{lam} = 1$ . The computed results of the  $B$  components in tangent and normal directions of  $H$  are compared with the numerical experiment data in Fig. 4. For the sake of easy comparison, the computed results by the elliptical model in [1] are also given in Fig. 3. It can be seen that the proposed model is much more accurate than the

elliptical model.

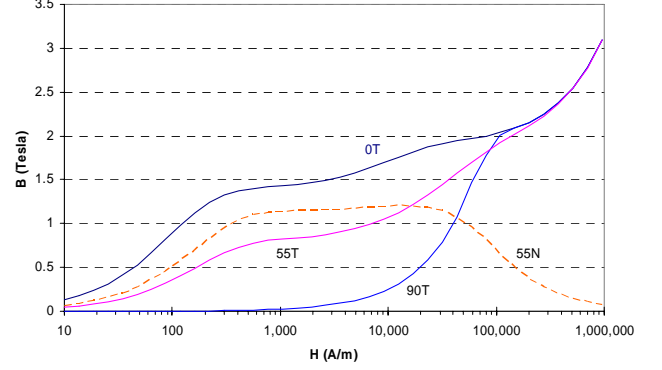


Fig. 3 Numerical results applying magnetic field at  $0^\circ$ ,  $55^\circ$  and  $90^\circ$  directions in M-15 non-oriented steel. T and N denote the tangential and normal directions, respectively.

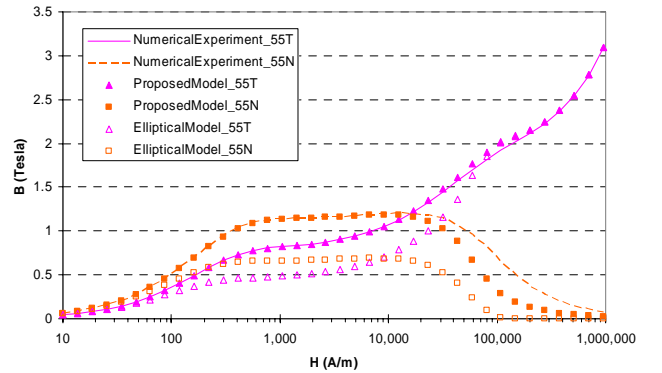


Fig. 4 Comparison between the numerical experiment and the computed results by the proposed model and the elliptical model

#### V. APPLICATIONS

As an application example, Fig. 5 displays a 400W 4-pole synchronous reluctance motor with axially-laminated anisotropic rotors.

For easy material property assignment, it is more convenient to use a cylindrical coordinate system fixed to the rotor. In such a case, the lamination direction (the normal direction) is in the radial direction  $r$  as shown in Fig. 5. Due to the periodic and symmetric conditions, one-eighth of the arrangement is analyzed.

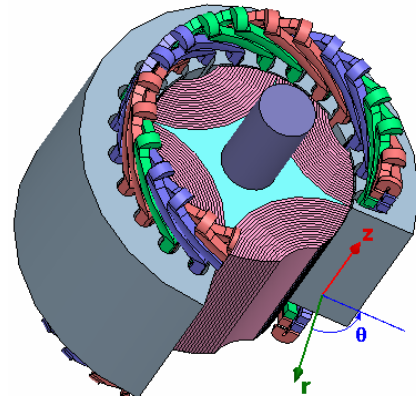


Fig. 5 The structure of a 400W 4-pole synchronous reluctance motor with axially-laminated anisotropic rotor

A three-phase 110V, 60Hz voltage source is applied to the three-phase winding of the motor, creating a rotating field with synchronous speed of 1800rpm. The air-gap torque at rated source voltage varying with the torque angle  $\theta$ , as shown in the phasor diagram of Fig. 6, is computed based on the slip method. Here, the rotor rotates at a speed a little lower than the synchronous speed. In this example, the rotor runs at 1650rpm. The performance of the motor is analyzed in one slip period, from 0 to 0.2 second, corresponding to 5Hz slip frequency.

The computed three-phase input currents are shown in Fig. 7. The current amplitude varies between 2A and 6A, corresponding to rotor positions when the  $d$  axis aligned with or perpendicular to the rotating field axis, respectively. The  $d$ -axis and  $q$ -axis reactances,  $x_d$  and  $x_q$ , can be derived from the ratio of the winding flux linkage to the winding current at these two special positions. Table I shows the computed results of  $x_d$  and  $x_q$ . Notice that  $x_d$  and  $x_q$  are nonlinear, and the values are only valid for a certain condition. The magnetic field distribution for the  $x_d$  computation is shown in Fig. 8.

The computed air-gap torque varying with the torque angle is shown in Fig. 9. We can see that the torque is not zero when the torque angle is zero. This is due to the effects of the stator winding resistance. We can also observe that the computed torque curve includes harmonics due to the effect of slots at slip operation. In reality, the curve is smoother because the average torque is derived over one period at the synchronous speed. The real torque curve can be obtained by field analysis at synchronous speed for various torque angles. Of course, this increases the computation time.

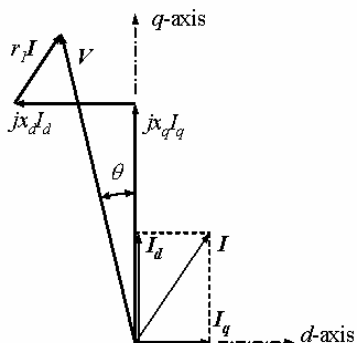


Fig. 6 The phasor diagram of synchronous reluctance motors

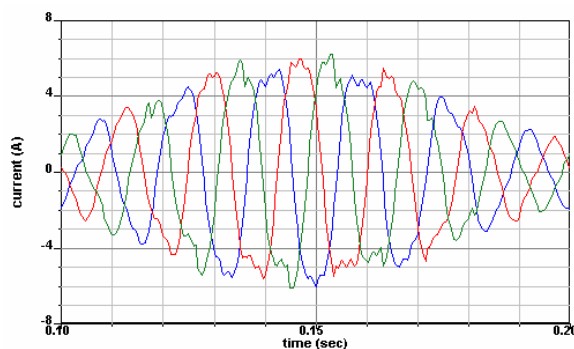


Fig. 7 Three-phase input current waveforms when the rotor rotates with a slip of 150rpm

TABLE I. COMPUTED D-AXIS AND Q-AXIS REACTANCES

$x_d$	$x_q$
77.0 ohms	25.6 ohms

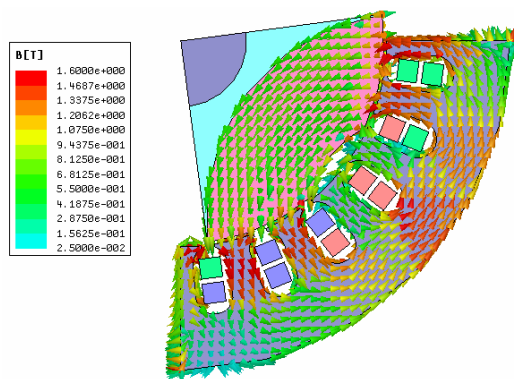


Fig. 8 The  $d$ -axis magnetic field distribution

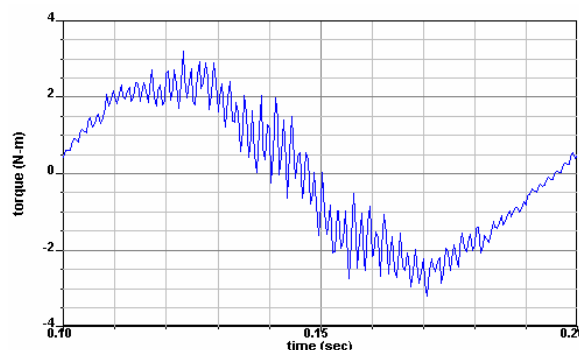


Fig. 9 Computed air-gap torque varying with the torque angle. The torque angle varies from 0 to 180 electric degrees as time changes from 0.1 to 0.2s.

## VI. CONCLUSION

This paper presents a new nonlinear anisotropic model for soft magnetic materials. The model requires only two or three  $B$ - $H$  curves in the principal directions depending on whether we perform the analysis in 2D or 3D. A further advantage is that these curves are directly available from the manufacturers. The validation by numeric experiments shows that the new model is more accurate than the elliptical model in [1]. Finally, the basic concepts of the nonlinear anisotropic

material model introduced in this paper can also be applied to treat the anisotropy of magnetic materials with hysteresis.

#### REFERENCES

- [1] J. M. Dedulle, G. Meunier, A. Foggia, J. C. Sabonnadiere, "Magnetic Fields in Nonlinear Anisotropic Grain-Oriented Iron-Sheet," *IEEE Transactions on Magnetics*, vol. 26, no. 2, pp. 524-526, March 1990.
- [2] P. P. Silvester, R. P. Gupta, "Effective Computational Models for Anisotropic Soft B-H Curves," *IEEE Transactions on Magnetics*, vol. 27, no. 5, pp. 3804-3807, September. 1991.
- [3] Jin Liu, A. Basak, A. J. Moses, G. H. Shirkoohi, "A Method of Anisotropic Steel Modeling Using Finite Element Method with Confirmation by Experimental Results," *IEEE Transactions on Magnetics*, vol. 30, no. 5, pp. 3391-3394, September 1994.
- [4] J. P. A. Bastos, G. Quichaud, "3D Modelling of A Non-Linear Anisotropic Lamination," *IEEE Transactions on Magnetics*, vol. 21, no. 6, pp. 2236-2369, November 1985.